Oxygen Stable Isotopic Analysis of Calcite by Raman Microprobe Spectrometry

by

Scott R. Mutchler

Thesis submitted to the faculty of Virginia Polytechnic Institute and State University in partial fulfillment of the requirements of the degree of

MASTER OF SCIENCE
in
GEOLOGICAL SCIENCES

APPROVED:

Robert J. Bodnar
Chairman

Robert C. Burruss

G. V. Gibbs

April, 1995
Blacksburg, Virginia

Oxygen Stable Isotopic Analysis of Calcite by Raman Microprobe Spectrometry

by

Scott R. Mutchler

Robert J. Bodnar, Chairman

Department of Geological Sciences

(ABSTRACT)

The oxygen stable isotopic compositions of minerals give valuable insight into the processes that govern many low- and high-temperature geologic systems. Much research has focused on the ability to analyze the fine scale oxygen isotopic zonation in many minerals using techniques such as the laser probe and ion microprobe. In this study I examine the feasibility of making high-resolution, nondestructive oxygen stable isotopic analyses with precision comparable to current microbeam techniques (i.e. <1‰) .

Five natural and two synthetic ^{18}O doped calcites were analyzed using the laser Raman microprobe (LRM) to determine whether the intensity ratio of the $C^{18}O^{16}O_2^{2-}$ and $C^{16}O_3^{2-}$ symmetric stretching bands can be directly related to isotopic compositions measured by ratio mass spectrometry (RMS). The calcites were cooled to near liquid nitrogen temperatures (78-90K) to remove the background from Mn^{2+} fluorescence and minimize the overlap of the symmetric stretching bands. At near liquid nitrogen temperatures the presence of the $C^{18}O^{16}O_2^{2-}$, $C^{17}O^{16}O_2^{2-}$, and $C^{16}O_3^{2-}$ symmetric stretching bands are clearly visible.

Initially LRM isotopic values showed poor correlation with RMS isotopic values;

however, the difference between LRM and RMS isotopic values was shown to be a linear function of the halfwidth of the symmetric stretching band. Corrected LRM isotopic values for all of the natural calcites agree with RMS values to within 3.8‰.

Currently the precision and accuracy of LRM isotopic measurements on calcite are several times poorer than for RMS measurements. The major limitation on the precision of the measurements is counting statistics. The strong Mn^{2+} fluorescence background of many natural calcites may also be a limiting factor on the precision of LRM isotopic measurements. However, the use of alternate laser excitation wavelengths and analysis at lower temperatures may allow Mn^{2+} fluorescence background to be eliminated in these calcites.

Acknowledgments

I would like to thank the members of my committee: Bob Bodnar, Bob Burruss, and Jerry Gibbs for their support and guidance during the course of this work. Bob Bodnar, Jerry Gibbs, Monte Boisen, and Cahit Çoruh are also thanked for their financial support of my research. Many others in the Department of Geological Sciences have also contributed greatly to this work. Without the technical knowledge and patience of Frank Harrison the success of this study would not have been possible. Todd Solberg has also contributed greatly with his time and insightful analytical strategies. I also would like to thank Kevin Rosso for being a sounding board for many of my ideas and general ramblings on Raman spectroscopy. Lastly, I would like to thank my family for their loving support throughout my educational career and of course none of this work would have been possible without the loving and constant support of my wife, Tara.

Table of Contents

List of Figures

List of Tables

Introduction

Oxygen and carbon stable isotopic compositions can provide valuable information on the origin and history of many geological materials. In particular, oxygen stable isotopic compositions have been valuable in determining the sources of fluids in many geologic environments (Sheppard and Taylor, 1974), for inferring paleoclimatic conditions (Mook, 1971), and for determining temperatures of geologic processes (O'Neil and Clayton, 1964). Because of the widespread applicability of oxygen isotopic compositions to the study of geologic systems, much research has focused on the development of analytical techniques which can accurately measure the oxygen isotopic compositions of geologically important materials.

Early measurements of the oxygen isotopic compositions of minerals were limited to measurements of bulk isotopic compositions using ratio mass spectrometry (RMS). While these measurements have been useful in studying many systems, it is clear that some minerals are visibly zoned and are neither chemically or isotopically homogeneous. With the recent ability to do high-spatial resolution analysis of stable oxygen isotopes in carbonates and silicates by techniques such as the ion microprobe and laser probe (Smalley et al., 1989; Riciputi and Paterson, 1994), oxygen isotopic zonations have been shown to occur in minerals on the scale of a few μm (Dickson et al., 1990). These techniques have replaced the mechanical sampling of traditional RMS analyses with sampling by an ion beam and laser beam, respectively. Currently, laser probes are capable of analyzing spot sizes of a few hundred micrometers with a precision of ≈ 0.4‰ (Smalley et al., 1989), while the ion

microprobe is capable of analyzing spots less than 30μm with an external reproducibility of 0.6‰, 1s (Riciputi and Paterson, 1994). The fine spatial resolution of these techniques has made it possible to indirectly measure the effect of changes in environmental conditions on increasingly small zonations in many minerals.

It has recently been suggested that high spatial resolution oxygen isotopic measurements may also be achieved by laser Raman microprobe (LRM) measurements (Burruss et al., 1989). The ability to measure isotopic variations by LRM would offer two major advantages over current microbeam techniques. The LRM offers nondestructive analysis with a spatial resolution an order of magnitude better than other current techniques (≈1μm). Analysis by LRM has the obvious advantage that the analyzed area can be further analyzed by other techniques such as with the electron microprobe or with various destructive techniques such as the ion probe, etc. The use of an electron microprobe and LRM would allow both trace element and oxygen isotope analyses to be obtained from zoned minerals with considerably better spatial resolution. In this study, we examine the feasibility of making oxygen isotopic measurements of calcite with geologically useful precision (i.e. <1‰) using LRM.

Previous Work

Raman spectroscopy is a vibrational spectroscopic technique. As such, changes in the mass of a molecule due to isotopic substitution can result in a change in the frequency of vibration for a given vibrational mode. This is referred to as isotopic splitting. The

isotopic splitting of Raman bands is a well known phenomenon (Herzberg, 1945). The position of the isotopic peaks for a particular vibrational mode can be calculated from the masses and arrangement of the atoms within a molecule. Moreover, the intensity of a peak for a given molecule is proportional to the concentration of the particular isotopic molecule and is discussed in detail below. In principle, one should be able to use the intensity ratio of two isotopic peaks for a given vibrational mode to determine the isotopic composition of a compound. The first attempt to use the intensity of Raman bands to measure isotopic variation in a material at the level of RMS was for liquid CO_2 (Rosaco et al., 1975 and Dhamelincourt et al., 1979). These studies reported precisions of 10-37‰ for $^{13}C/^{12}C$ in liquid CO_2 fluid inclusions. The precision of this earlier study is much less than the precision of routine RMS measurements (i.e. <0.5‰). Burruss et al. (1989) later examined the $^{13}C/^{12}C$ ratio in fluid inclusions using a multichannel LRM instrument. The precision of the measurements in that study was within the range of the earlier measurements (±24.5‰). In addition to CO_2, Burruss et al. also examined the symmetric stretching band of the carbonate group in calcite. This band is ideal for intensity measurements due to the symmetric stretching bands intense Raman scattering. The presence of the $C^{18}O^{16}O_2^{2-}$ peak is easily distinguished from the more intense $C^{16}O_3^{2-}$ peak. Burruss et al. attempted to "calibrate" LRM intensity ratios with RMS isotopic values. However, observed intensity ratios of the $C^{18}O^{16}O_2^{2-}$ peak to the $C^{16}O_3^{2-}$ peak yielded a poor correlation with RMS measured values. He pointed to Mn^{2+} fluorescence background and instrumental limitations as limiting factors in determining isotopic ratios using LRM (Burruss et al., 1990). Large

variations in the intensity ratio measured by LRM were observed which were at least an order of magnitude larger than those predicted by counting statistics. Further work by Erickson et al. (1991) found that some of this variance may be ascribed to translational disorder of the carbonate ion, which can be related to broadening of the symmetric stretching peak, increasing cell volume, and decreasing mol% Ca. Corrected $\delta^{18}O$ values for five of the calcites in that earlier study were within 5.6‰ of those measured by ratio mass spectrometry (RMS), while two others disagreed by 92.1‰ and 232.1‰. Although the results of this earlier study were encouraging, they also suggested that the precision and accuracy of LRM $\delta^{18}O$ measurements are limited to several times poorer than the precision and accuracy of RMS measurements. However, the recent development of high signal-to-noise CCD detectors and the ability to make routine measurements at low temperatures offer an opportunity to improve the precision and accuracy of such measurements to be comparable with RMS measurements.

Experimental Procedure

To test the feasibility of conducting meaningful oxygen isotopic analyses of calcite, both natural and synthetic calcites were analyzed. Thirty-eight calcite samples were examined using LRM to measure the intensity of Mn^{2+} fluorescence. In order to minimize fluorescence background in LRM measurements, the calcite samples chosen for analysis which exhibited little to no Mn^{2+} fluorescence background at room temperature. Moreover, the samples were analyzed at low temperatures to further reduce any Mn^{2+} fluorescence

background. Low temperature measurements allowed complete removal of fluorescence background in the LRM spectra of the calcites examined. In an attempt to "calibrate" LRM intensity measurements with RMS isotopic values, each sample was analyzed by RMS. In the absence of natural materials with large isotopic variabilities, synthetic ^{18}O-doped calcites were also analyzed by RMS. The bulk isotopic measurements of the natural and synthetic calcites were then correlated with LRM intensity measurements of the $C^{18}O^{16}O_2^{2-}$ and $C^{16}O_3^{2-}$ symmetric stretching peaks.

Analyses were carried out on five polished cleavage fragments of natural calcite crystals and two ^{18}O-doped synthetic calcite powders. The ^{18}O-doped calcite powders were prepared using the procedure described by Cloots (1991). Ca metal (≈ 0.1g, 99.99% purity) was reacted with an excess of ^{18}O-doped water (purchased from Isotec, inc.). The resulting $Ca(OH)_2$ solution was then reacted with CO_2 of normal isotopic composition. The precipitate was isolated by drying and sealed under vacuum in a silica tube which was placed into an oven at 800°C for 7 days to improve crystallinity. Two separate runs resulted in calcite powders with isotopic values of 6,258.8‰ and 23,658.9‰ from starting solutions of 2.14% and 8.56% ^{18}O, respectively. The isotopic composition of the powders was determined using conventional ratio mass spectrometric techniques. The powders were then pressed into pellets for analysis.

Past research has shown that the background fluorescence produced by trace amounts of Mn^{2+} in calcite is one of the major limitations in determining oxygen isotopic compositions with LRM (Burruss et al., 1989; Burruss et al., 1990; Erickson et al., 1991).

Because it is well known that the fluorescence spectrum of Mn^{2+} in calcite narrows significantly at low temperatures (Walker et al., 1989), which results in less fluorescence background in the region of interest in this study, all analyses were conducted at near-liquid nitrogen temperatures in a Joule Thompson N_2 cooling stage (MMR Technologies, Inc.). Cleavage fragments and pressed pellets were secured onto a polished wafer of pyrolitic graphite (cut $\perp$ to the *c* axis) using a thermally conductive paste. The paste was only placed under one corner of the fragment, due to the fact that the paste is strongly fluorescent. The use of pyrolitic graphite allowed for a high degree of thermal conductivity between the sample and cooling stage and also contributed negligible background to the LRM measurements. Analyses were conducted on samples cooled to 78-90 K. Cooling to 78 K was not possible in all runs due to laser heating of the cooling stage. Raman spectra were collected using a Dilor XY modular laser Raman spectrometer with a 0.64 m focal-length foremonochromator in high dispersion mode. The spectrometer is coupled with an Olympus BH2 optical microscope. The resulting beam spot, using the 514.5 nm line of an argon-ion laser and 80× (NA = 0.75) objective, was approximately 0.8μm in diameter with a depth of focus of 3.6μm (Adar, 1981). The Dilor XY is equipped with a multichannel, Peltier-cooled OMA4 CCD detector (EG&G instruments) with a 1024 × 256 element array. All spectra were collected over the range 926-1269 cm^{-1} with a 400μm entrance slit giving a spectral resolution of 0.3 cm^{-1}. The entrance slit width represents a compromise between spectral resolution and the signal to noise ratio. The laser power was set at 500 mW (70 mW at the surface of the sample) for all runs, and a total of 1 hour and 40 minutes acquisition

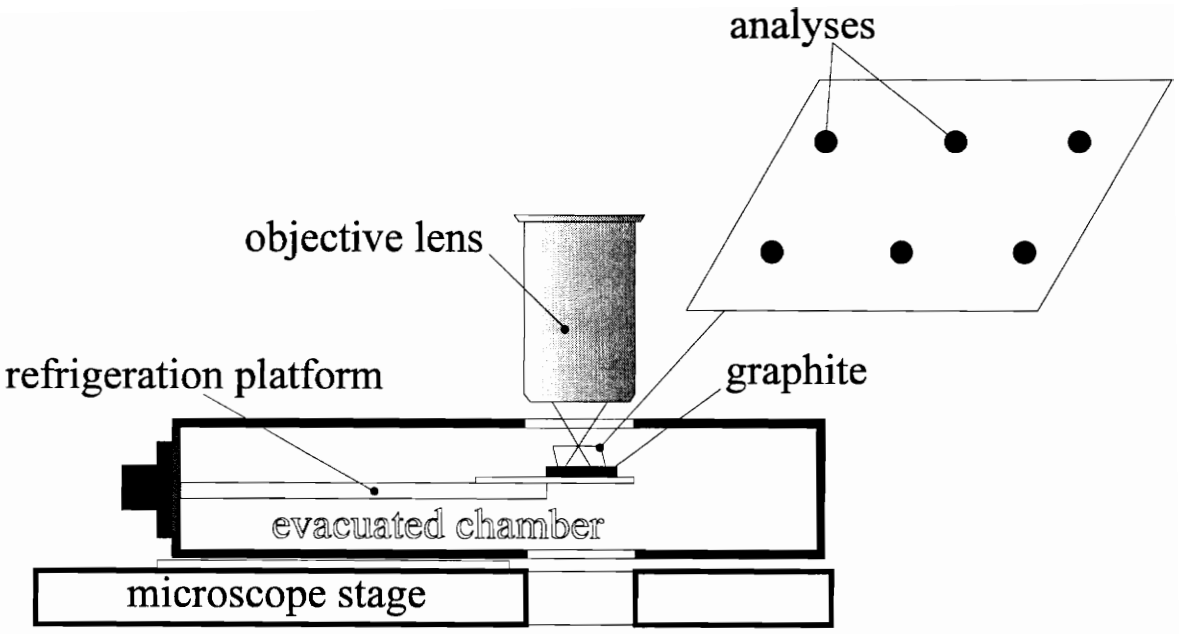

Figure 1: A schematic representation of the experimental setup for the LRM measurements in this study.

time was required for each spectrum (an average of 50 spectra at 2 minutes/spectrum). This acquisition time was chosen to allow several evenly spaced spots along the surface to be analyzed within a daily acquisition period. The average value for these spots was then related to the bulk RMS isotopic value for the sample. A minimum of six distinct points, separated by 3mm to 6mm, on each fragment were analyzed.

Two separate external measures of instrumental drift were employed to determine the magnitude of daily variations in detector response and any scaling of true intensity ratios due to the wavelength dependence of the detector response. First, a single sample (HB659) was analyzed daily on a distinct spot (±5μm). Comparison of the observed and theoretical variances in intensity ratios for a single spot was used to determine if any additional variance was due to detector response. Second, the spectrum of a calibrated W-lamp was recorded over the analysis range daily. The W-lamp is a known black-body emitter which has a characteristic emission spectrum for a given black-body temperature. This makes it ideal for determining the wavelength dependence of the detector response. The black-body temperature was determined as a function of voltage across the lamp by use of an optical pyrometer (Strommen and Nakamoto, 1984). The spectra recorded daily were at a voltage of 2.4V which resulted in a black-body temperature of 2712 K. The ratio of the theoretical black-body emission spectra to the recorded spectra revealed that the intensity ratios in this study are scaled by less than 4% of their true values. Moreover, analysis of both W-lamp and the HB659 spectra revealed that there was no measurable variation in detector response at the level of our measurements. Due to the fact that the LRM isotopic ratios in this study

were determined relative to a standard (HB659), only variances between samples are important. Therefore, no correction for detector response was applied to the measured intensity ratios in this study.

All spectra were analyzed using Spectra Calc™ version 2.2 software. The symmetric stretching bands were fit using a peak composed of a sum of Gaussian and Lorentzian components using the maximum likelihood fitting program Fit™ version 1.4 from the Square Tools™ utilities package. Fit™ reported the following optimized parameters: peak centers, heights, halfwidths (fullwidth at half maximum), and fraction of Lorentzian character (Appendix II).

The Raman Spectrum of Calcite

The structure of calcite can be considered to be composed of an oriented molecule (H_2CO_3) within a periodic structure. In this model the carbonate ion retains the internal vibrations of the molecule, but has its rotational and translational freedom replaced by lattice vibrations, librations, and limited translational movement within the structure (Long, 1977). There are two carbonate groups within the unit cell related by an inversion center (Figure 2). The Raman active modes of vibration in calcite involve vibrations of the carbonate groups such that the symmetry of the inversion center is retained. There are four such internal and two external (lattice) vibrations in the Raman spectrum of calcite (Figure 3). The most intense Raman scattering is the result of the totally symmetric stretching mode (ν_1 after Herzberg, 1944) at approximately 1085 cm^{-1}.

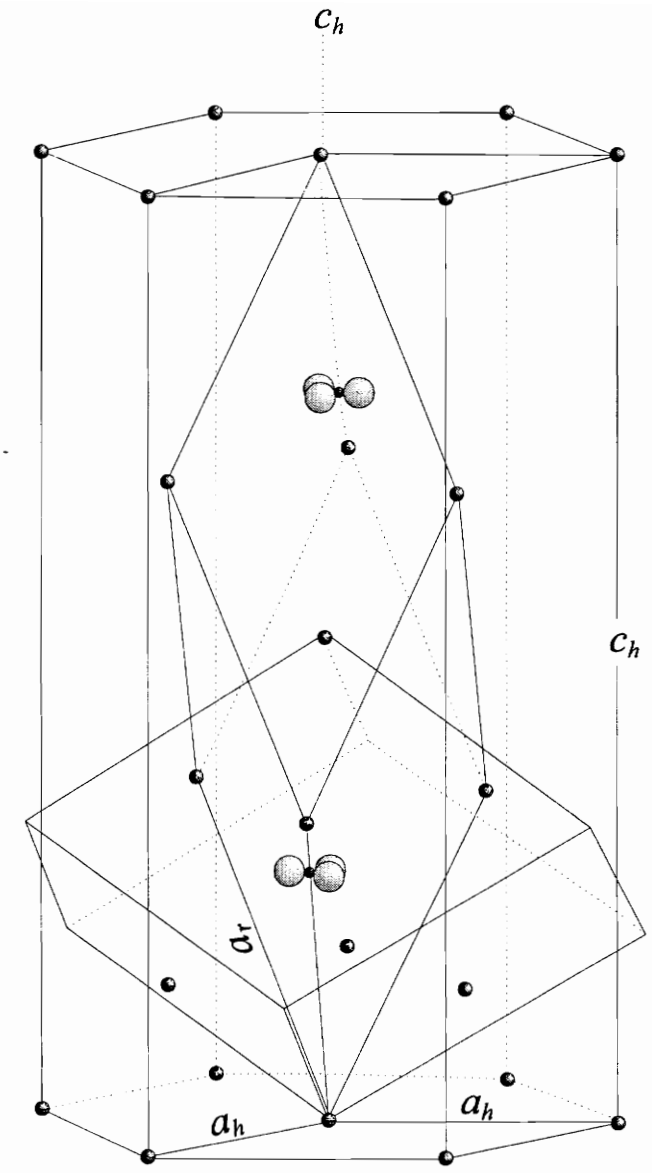

Figure 2: A schematic representation showing the relationship between the morphologic (cleavage), hexagonal, and rhombohedral (the acute rhobohedron) unit cells of calcite (after Hurlbut and Klein, 1977). The orientation of the two carbonate groups within the primitive rhombohedral unit cell are shown. The carbonate groups are related by an inversion center. Raman active modes of vibration preserve this inversion center while infrared active modes of vibration do not.

Internal Modes		Lattice Modes
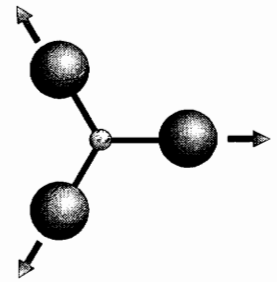	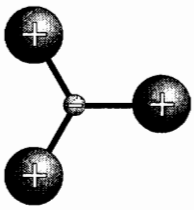	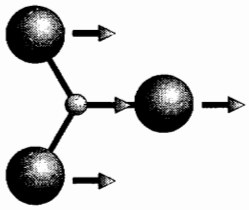
ν_1 (A_{1g})	$2\nu_2$ (A_{2u})	T (E_g)
symmetric stretch	out-of-plane bend	translation
1085 cm^{-1}	1748 cm^{-1}	154 cm^{-1}
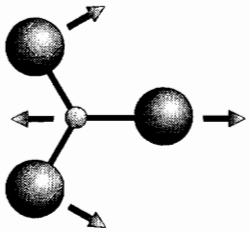	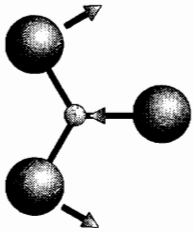	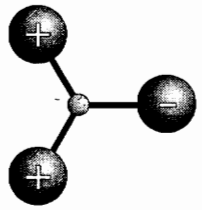
ν_3 (E_g)	ν_4 (E_g)	L (E_g)
antisymmetric stretch	in-plane bend	libration
1435 cm^{-1}	712 cm^{-1}	280 cm^{-1}

Figure 3: The Raman active vibrational modes of calcite (after White, 1974). There are four Raman active internal modes of vibration, which involve only the motion of the atoms in the carbonate group, and two Raman active lattice vibrations. The mode $2\nu_2$ is the second overtone of an infrared active mode of vibration. Notice that the symmetric stretching mode involves the symmetric displacement of the oxygen atoms, but not the central carbon atom.

Krishnamurti (1957) was the first to note weak satellite peaks to the symmetric stretching peak, occurring at 1067, 1072, and 1075 cm^{-1}. He attributed them to a splitting of ν_1 due to vibrational coupling between ν_1 and inactive modes of vibration. Cloots (1991) has shown, however, that the presence of the satellite at 1067 cm^{-1} (denoted ν_1*) is due to the presence of $C^{18}O^{16}O_2^{2-}$ and is present in carbonates with both the aragonite and calcite structure types. Reexamination of the Raman spectrum of the carbonate ion in solution (White, 1974) also showed this satellite to be present, although both peaks occur at lower wavenumbers than in calcite. This satellite peak can only be attributed to isotopic substitution by oxygen and not carbon. The symmetric stretching mode involves only the displacement of the oxygen atoms (Figure 3). Therefore, changes in the mass of the carbon atom do not affect the vibrational frequency of the ν_1 mode, but the larger mass of the ^{18}O or ^{17}O atom causes a slight decrease in the vibrational frequency, thereby splitting ν_1 into a total of three peaks. Because the ν_1 vibration mode only involves a stretching motion, the vibrational frequency can be approximated by an harmonic oscillator. In the harmonic oscillator approximation

$$\nu = \frac{1}{2\pi}\sqrt{\frac{f_{C\text{-}O}}{m_O}} \qquad (1)$$

where ν is the frequency of the symmetric stretching vibration, $f_{C\text{-}O}$ is the C-O force constant, and m_O is the mass of the oxygen atom. Using this equation the effect of isotopic substitution, or change of mass, on the vibrational frequency can be determined. The

approximate ratio of isotopic frequencies for ^{18}O substituting for ^{16}O should be

$$\frac{\nu^*}{\nu} = \sqrt{\frac{16}{18}} \approx 0.94 \qquad (2)$$

and 0.97 for ^{17}O substituting for ^{16}O in the carbonate group. The actual degree of splitting in calcite is, however, somewhat smaller: 0.98 and 0.99 for ^{18}O and ^{17}O respectively. However, the splitting due to ^{18}O in the carbonate ion in solution is 0.95 (White, 1974), in good agreement with the predicted value. The decreased splitting in calcite, compared to the "free ion", can be explained by considering the assumptions inherent in the use of equation (1). The relationship in equation (1) holds only if: 1) the C-O force constant remains unchanged with the change of mass of the oxygen atom; 2) the vibrational motion is *pure* and is not coupled with other vibrational modes. The first is a reasonable assumption because the addition of one or two neutrons should not change the electronic distribution of the bond to a first approximation (Diem, 1994). However, it is possible that there is some degree of coupling of ν_1 with another mode of vibration in calcite that accounts for experimental splitting being smaller than is calculated. This type of coupling has been observed for nitrates and for $BaCO_3$ (Decius, 1954; 1956).

The intensities of Raman bands (peak heights or areas) can be expressed as

$$I \propto \nu^4 f(\alpha^2) N I_0 \qquad (3)$$

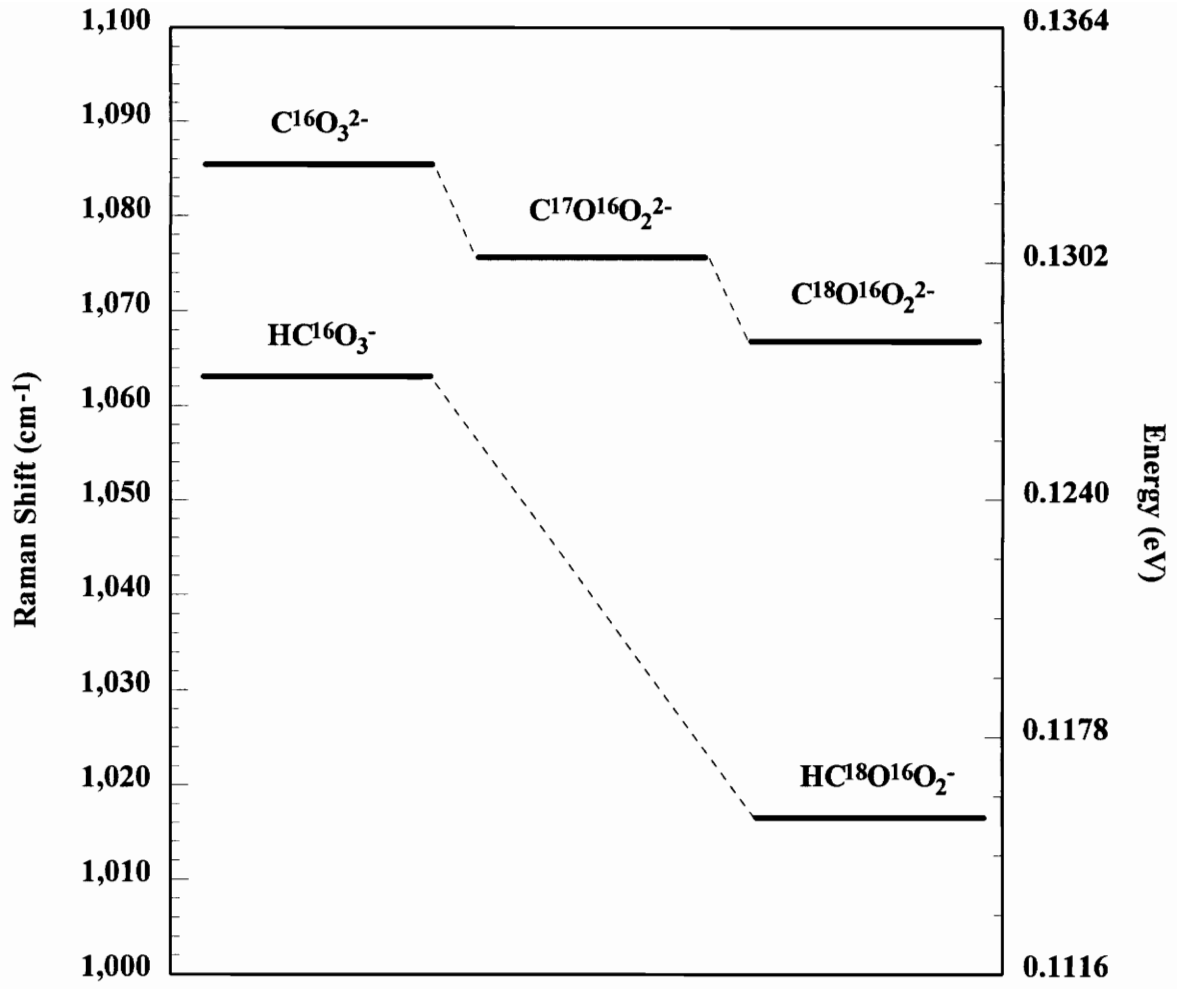

Figure 4: Energy level diagram for the isotopic splitting of the ν_1 vibrational mode of the carbonate group in calcite (top) and in solution (bottom). Data for the carbonate group in solution are for a 1M aqueous solution of Rb_2CO_3 (White, 1974). The position of the $HC^{17}O^{16}O_2^-$ band was not visible in the Raman spectrum of the Rb_2CO_3 solution due to its inherent weakness and proximity to the more intense $HC^{16}O_3^-$ band.

where ν is the frequency of the exciting light (in s^{-1}), N is the number of molecules in the excitation volume, I_0 is the intensity of the exciting light, and α is the polarizability of the sample (Diem, 1994). The functionality of the polarizability of the sample is determined by the directions of excitation and observation of the Raman scattering. To understand this function we must first look at the polarizability (expressed as a tensor) for the normal mode of vibration that gives rise to a Raman band. For the symmetric stretching mode of the carbonate group in calcite, the polarizability tensor is given as

$$\alpha = \begin{bmatrix} \alpha_{xx} & 0 & 0 \\ 0 & \alpha_{xx} & 0 \\ 0 & 0 & \alpha_{zz} \end{bmatrix}. \qquad (4)$$

If a laser beam polarized along the *x*-axis is directed along the *z*-axis of a calcite crystal, and if the scattered radiation polarized along the *x*-axis is observed along the *y*-axis (denoted $z(xx)y$), the scattering intensity would be proportional to α_{xx}^2. Thus changing the orientation of the sample may change the intensity of the symmetric stretching band. However, due to the fact that the isotopically substituted band (ν_1*) arises from the same vibrational mode as the "normal" band (ν_1), the intensities of the bands should remain at a constant ratio regardless of orientation. This assumption rests on the fact that the polarizability of the mode does not change with isotopic substitution (Herzberg, 1945). The intensity ratio of ν_1*/ν_1 then can be reduced to

$$\frac{I_{\nu_1^*}}{I_{\nu_1}} = \frac{N^*}{N} \quad . \tag{5}$$

Given this, the intensity ratio of ν_1^*/ν_1 should be a direct measure of the ratio of the number of $C^{18}O^{16}O_2^{2-}$ molecules to $C^{16}O_3^{2-}$ molecules. This ratio is approximately three times the absolute ratio of $^{18}O/^{16}O$. The intensity ratio of ν_1^*/ν_1 for *both* the ^{18}O and ^{17}O peaks determined experimentally is very close to three times the absolute ratio of $^{18}O/^{16}O$.

As pointed out by Burruss et al. (1990), measuring $\delta^{18}O$ values using the intensity ratio of ν_1^*/ν_1 at the level of routine RMS measurements (i.e. <1‰) requires the ability to measure very small changes in the intensity ratio of ν_1^*/ν_1. The relationship between $\delta^{18}O$ values, reported in per mil notation (‰), and the absolute ratio of $^{18}O/^{16}O$ is given by

$$\delta^{18}O = \left(\frac{R_{smp} - R_{std}}{R_{std}} \right) \times 10^3 \quad , \tag{6}$$

where R_{smp} and R_{std} are the absolute ratios of the sample and standard, respectively. Thus a 1‰ variation is only a one part in one thousand variation in the absolute ratio. Measurements of this sensitivity are approaching the technological limits of what is possible even with recent advances in multichannel detector technology. Most reports of quantitative Raman measurements are given for single-channel Raman instruments. Detection limits for such instruments are on the order of 1:100 to 1:1000 with precisions of about 1% relative (Hirschfield, 1982; Pasteris et al.,1988).

The ability of RMS to routinely measure variations of less than 1‰ is made possible by the simultaneous analysis of sample and standard. Variations in instrumental conditions that might otherwise result in large variations in measured values are effectively nullified by this ratioing technique. Similar analyses are not yet possible with the LRM where analyses are limited to one sample at a time. The use of multichannel detectors does, however, permit much of the variation in peak intensities resulting from fluctuations in laser power to be eliminated by collecting the signal for all peaks simultaneously. The limiting factor, however, in quantifying such small variations in ratioed intensities is that of counting statistics.

The importance of counting statistics can be seen by evaluating the total variance in the intensity of a Raman peak. The total variance can be approximated as

$$s_t^2 \approx s_p^2 + s_b^2 + s_f^2 \tag{7}$$

where s_t^2, s_p^2, s_b^2, and s_f^2 are the total, peak, background, and peak fitting variances, respectively. The intensity of a Raman peak is determined by photon counting and thus is governed by the Poisson distribution. This distribution has the property that the variance in the number of photons counted is simply equal to the number of photon counts (n),

$$s^2 = n \ . \tag{8}$$

The total counts for each peak is composed of two separate distributions. The first is the background, caused by detector "dark current" and any Mn^{2+} fluorescence. The majority of the counts are due to Raman scattering. Second, there are errors inherent in fitting the spectra and removal of any baseline. Figure 5 shows the error in the peak ratio in per mil as a function of integration time for various laser intensities using the LRM instrument described above. Calculation of required integration times reveals that analysis with a precision comparable to other current microbeam techniques is theoretically possible, but the time required is significantly greater.

Results & Discussion

Examination of the Raman spectra of the natural calcites analyzed in this study clearly shows the presence of the $C^{16}O_3^{2-}$, $C^{17}O^{16}O_2^{2-}$ and $C^{18}O^{16}O_2$ symmetric stretching peaks (Figure 6). The presence of the $C^{17}O^{16}O_2^{2-}$ peak was not noted in many earlier published Raman studies of calcite due to its low intensity and proximity to the much more intense $C^{16}O_3^{2-}$ peak. Cooling the samples to near liquid nitrogen temperatures, however, results in a significant narrowing of the peaks in the Raman spectrum of calcite (Figure 7). The improved resolution at low temperatures made observation of the $C^{17}O^{16}O_2^{2-}$ peak possible in all of the natural calcites and also allowed intensity measurements of the $C^{17}O^{16}O_2^{2-}$ peak for three of the natural calcites. The symmetric stretching peaks for the remaining calcites were too broad to completely separate the $C^{17}O^{16}O_2^{2-}$ and $C^{16}O_3^{2-}$ peaks by peak fitting. Moreover, it was not possible to observe the $C^{17}O^{16}O_2^{2-}$ peak in spectra of

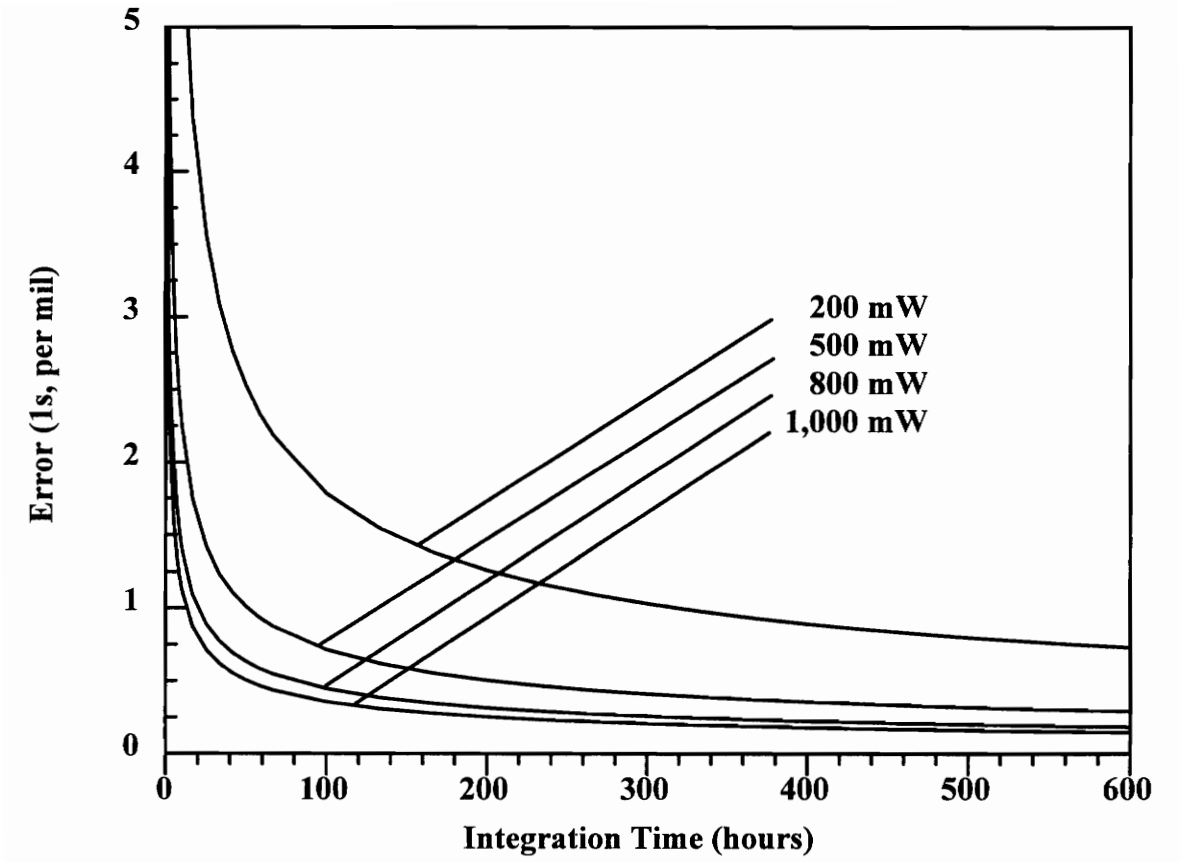

Figure 5: Theoretical error (1s) for LRM measurements of the intensity rato of ν_1^*/ν_1 as a function of integration time for various source laser powers for the LRM instrument in this study. The laser power at the sample is approximately 14% of the source laser power. Theoretical errors include a 1% error in intensities due to peak fitting. The error decreases with increasing laser power; however, high laser powers can cause significant heating of the sample. Heating results in an increase in the widths of the symmetric stretching peaks. As the widths of the symmetric stretching peaks increase it becomes increasingly difficult to separate the peaks by peak fitting methods.

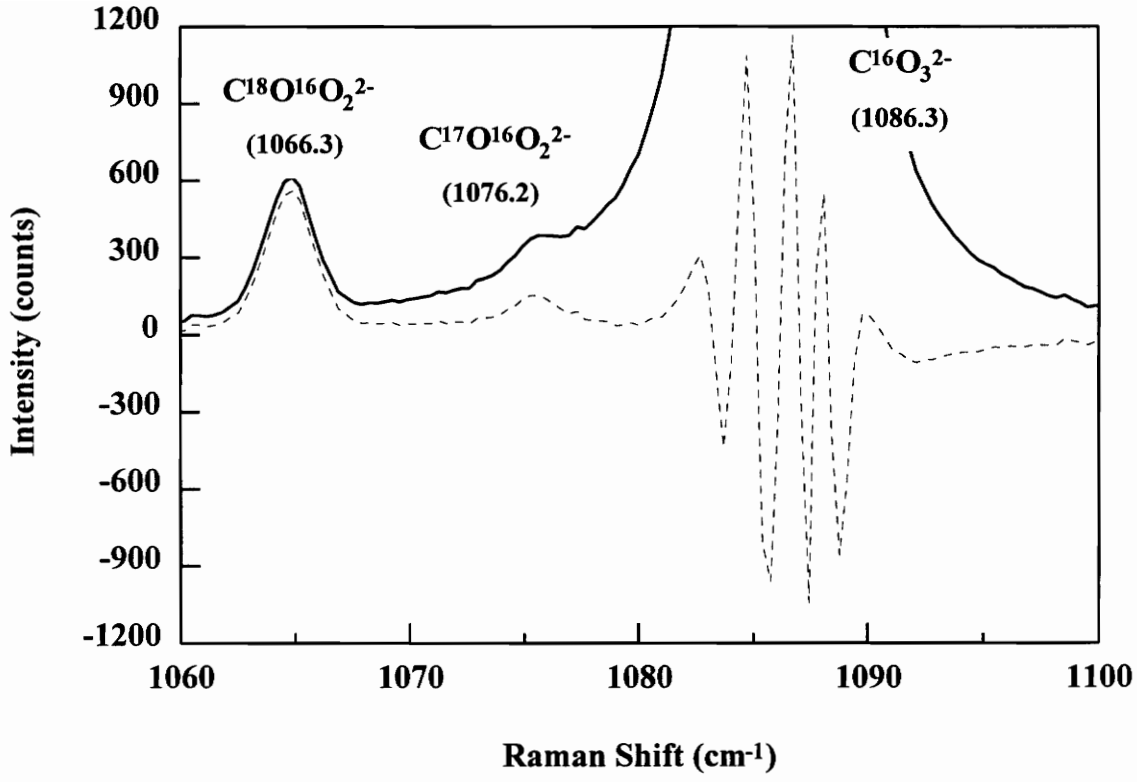

Figure 6: The Raman spectrum of a natural calcite sample, OB001 at 80K. The $C^{18}O^{16}O_2^{2-}$ and $C^{17}O^{16}O_2^{2-}$ peaks are clearly visible. The dotted line represents the residual of the spectrum after the $C^{16}O_3^{2-}$ peak is fit and subtracted out.

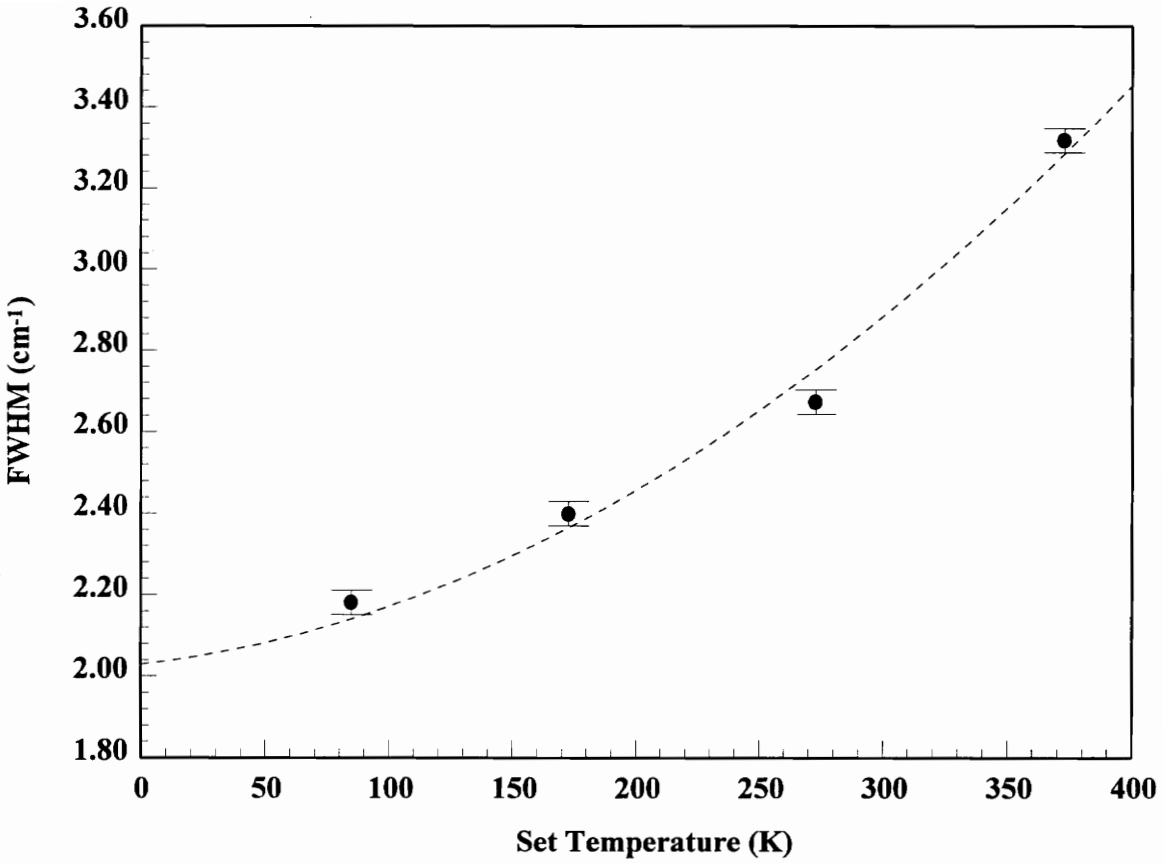

Figure 7: The effect of cooling on the halfwidth of the symmetric stretching peak in calcite (HB659). The halfwidth at a given temperature is also a function of the entrance slit width of the spectrometer, crystallinity of the sample, and substitution of trace elements for Ca^{2+}. Error bars represent three standard deviations from the mean. The dotted line is a second order polynomial fit.

the synthetic calcites due to the increased widths of the symmetric stretching peaks. The increased widths of the symmetric stretching peaks in the synthetic samples may be the result of increased crystallographic disorder (Bischoff et al., 1985) due to poor crystallinity. In addition to the narrowing of the symmetric stretching peak, low temperatures also have a marked effect on narrowing the fluorescence emission spectrum of Mn^{2+} in calcite (Figure 8). The narrowing of this fluorescence band is important because the symmetric stretching peak in calcite is located on the low wavenumber side of the Mn^{2+} fluorescence spectrum. Thus Mn^{2+} fluorescence can contribute greatly to the background in Raman measurements. The increase in background contributes to the error in intensity of the symmetric stretching bands (Equation 7). The narrowing of the Mn^{2+} fluorescence at 80K removes nearly all fluorescence background in a relatively weakly fluorescent sample (Figure 8). However, strongly fluorescent samples can still contribute a large amount of background to LRM measurements of the symmetric stretching peak. In the present study it was desirable to limit the effects of fluorescence on all measurements. Only LRM spectra where there was no fluorescence background were used for calculating intensity ratios.

The Raman spectra for the ^{18}O-doped calcites show an increased intensity ratio for ν_1^*/ν_1 when compared to the natural calcites (Figure 9). The intensity information for the two doped calcites was used to determine the relation between the LRM intensities and RMS isotopic values. Comparison of ν_1^*/ν_1 intensities with isotopic values measured by RMS for the two doped calcite powders reveals that there is a 6.0×10^{-6} variation in the intensity ratio/per mil. This corresponds to a variation in the intensity of ν_1^*/ν_1 for the natural

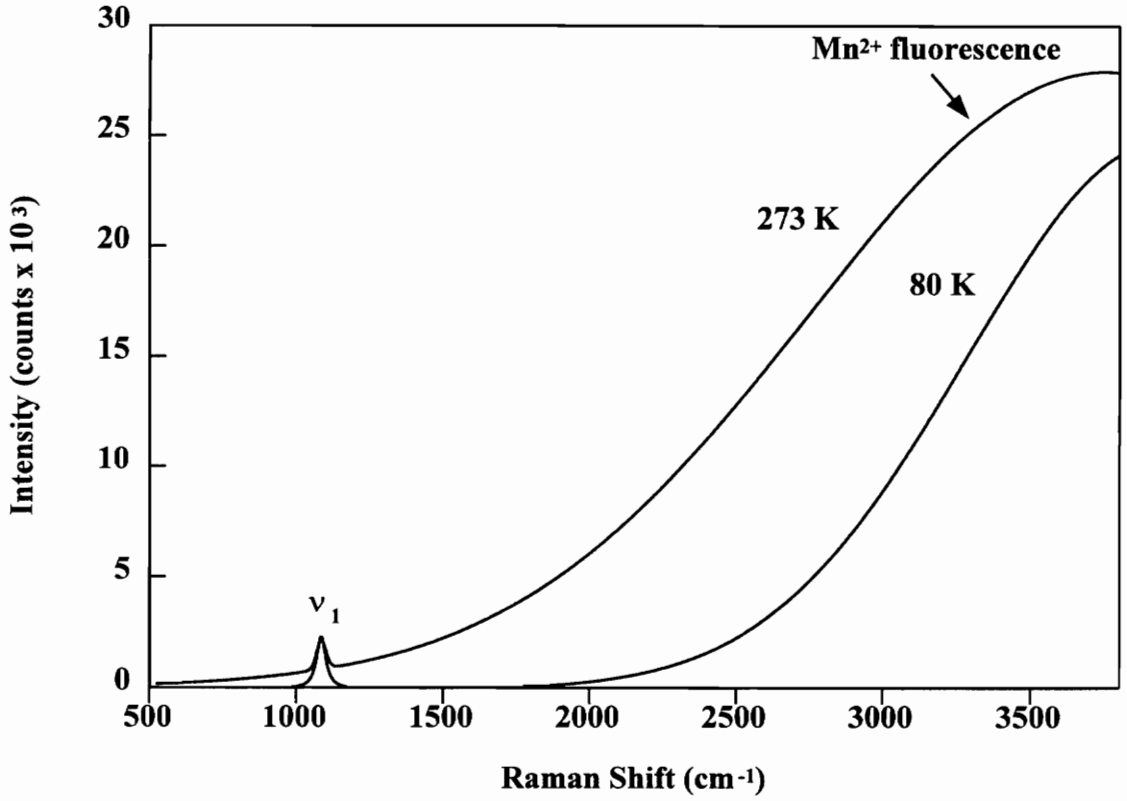

Figure 8: LRM fluorescence spectrum of a natural calcite, SF0232 at 80 and 273K. The width of the Mn^{2+} fluorescence band narrows by approximately 25% when the sample is cooled to 80K. The narrower fluorescence band results in less background in LRM measurements of the symmetric stretching peaks.

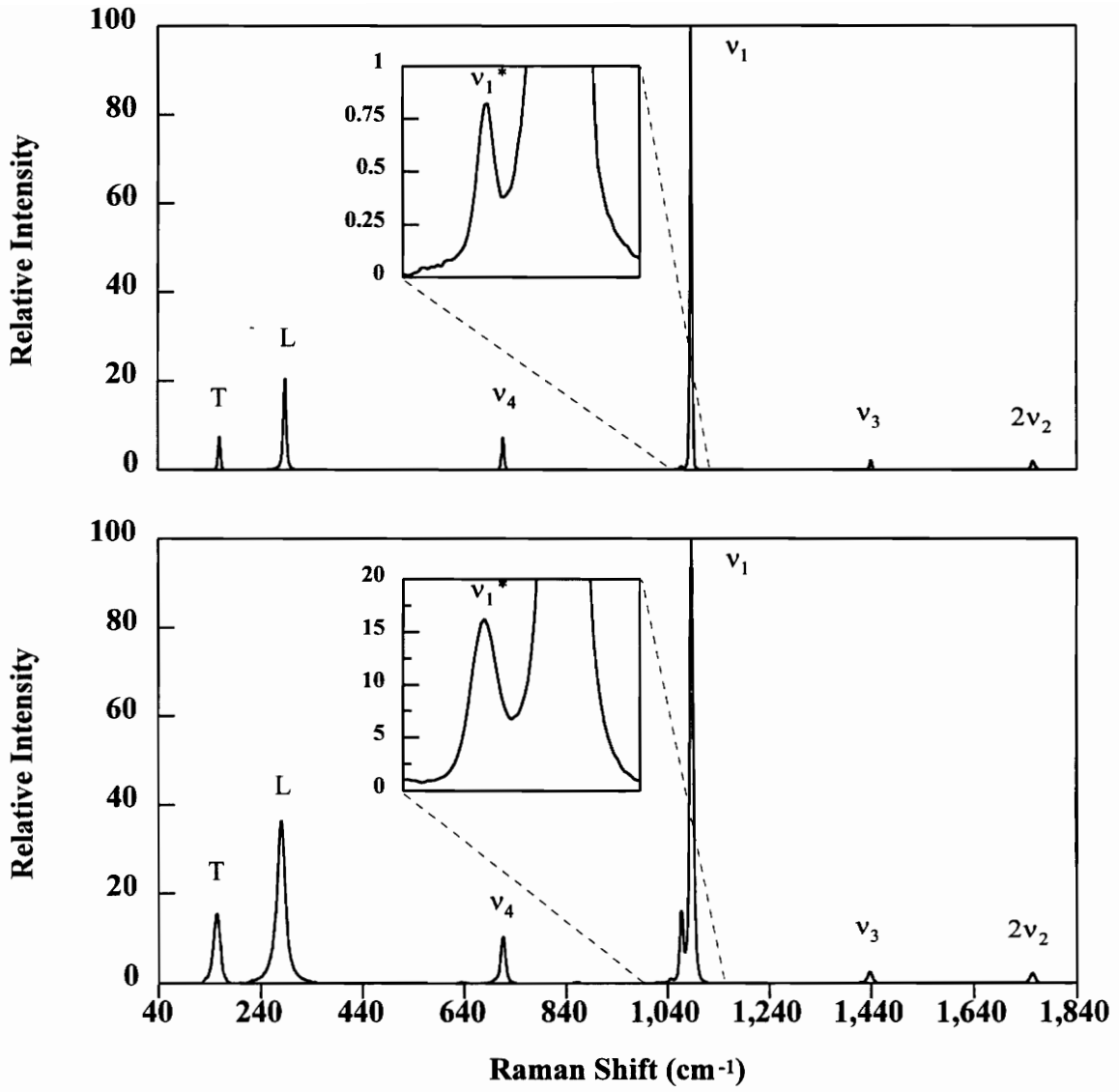

Figure 9: The Raman spectrum of a natural calcite, SF0232 (top) and an ^{18}O-doped synthetic calcite, SYN6 (bottom). Note the relative increase in intensity of the ν_1* in the synthetic calcites. The increase in width of all peaks in the lower spectrum is probably the result of the poor crystallinity of the synthetic calcite.

samples of about 1 part in a thousand. Using this fact, it was possible to recast the intensities of each of the samples in per mil relative to an arbitrary standard, HB659. At first the calculated LRM isotopic values showed a poor correlation with the RMS isotopic values. Further examination, however, showed that the differences in the values determined by LRM and those determined by RMS were a smooth function of the halfwidth of the symmetric stretching peak (Figure 10). This relationship was also observed by Erickson et al. (1991). Correction for the broadness of the ν_1 peak results in LRM isotopic values for all the natural calcites that are within 3.8‰ of those determined by RMS. Extending this model to the synthetic calcites yields $\delta^{18}O$ values that vary by approximately 1,500‰ over RMS values (see Table 1). The variances in the calculated $\delta^{18}O$ values for the natural samples are, in general, slightly larger than predicted (i.e. 6.7‰). However, for two of the samples (HB659, SF0232) the observed variances were slightly smaller than predicted. Much of the additional variance may be ascribed to error in baseline removal which could not be assessed in calculating theoretical variances.

The reason for the observed relationship between the increasing halfwidth of ν_1 and the increased ν_1^*/ν_1 intensity ratios is unknown. It is interesting to note that the halfwidths of all three isotopic bands of ν_1 were equal for every sample. This is not surprising considering the bands all arise from the same vibrational mode. However, the halfwidth of ν_1 varies considerably from one sample to another. The halfwidth of ν_1 is known to be a function of the temperature, the experimental slit width, the crystallinity of the sample, and the substitution of trace elements for Ca^{2+}. The halfwidth has been shown to increase

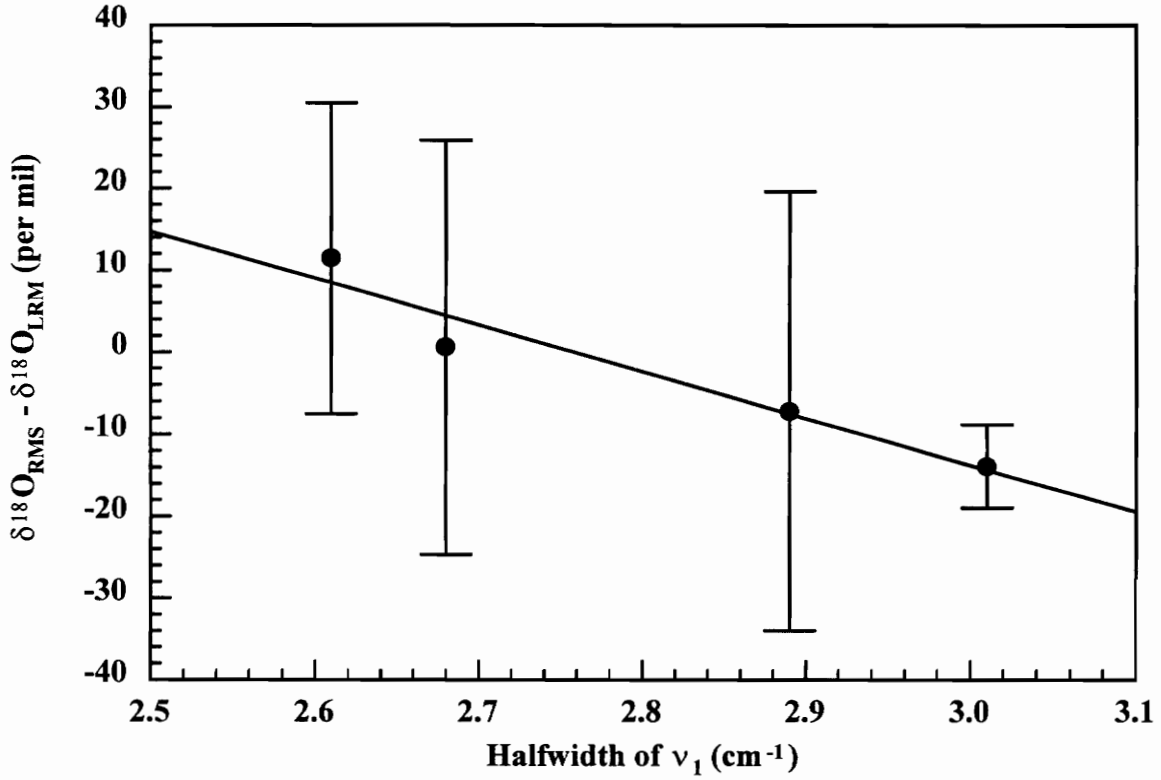

Figure 10: Graph showing the difference between RMS and LRM $\delta^{18}O$ values as a function of halfwidth of ν_1. The linear relationship between the halfwidth of ν_1 and the difference between RMS and LRM $\delta^{18}O$ values allows back calculation to $\delta^{18}O$ values within 3.8‰ of RMS values for the natural calcites in this study.

Table 1. Stable oxygen isotopic compositions determined by ratio mass spectrometry (RMS) and laser Raman microprobe spectrometry (LRM) for five natural calcites and two synthetic calcites.

Sample	Height Ratio (ν_1^*/ν_1)	Halfwidth of ν_1 (cm^{-1})	$\delta^{18}O$ RMS (‰, SMOW)	$\delta^{18}O$ LRM (‰, HB659)	s (‰, HB659)
HB659[a]	0.005977	2.63	17.4	—	5.7
C60686[b]	0.005972	2.89	9.3	9.0	26.8
OB001[b]	0.005959	2.68	15.0	18.8	25.3
VPI001[a]	0.005915	2.61	18.6	15.5	19.0
SF0232[a]	0.006094	3.01	23.0	22.6	5.1
SYN5[c]	0.034302	5.51	6258.8	4581.1	77.3
SYN6[c]	0.138909	5.48	23358.9	22017.3	116.9

a) Virginia Polytechic Institute & State University Museum of Natural History
b) American Museum of Natural History
c) Synthetic

linearly with increasing substitution of Mg^{2+} for Ca^{2+} in calcite (Bischoff et al., 1985). The increased halfwidth is the result of differences in the immediate cation neighborhood of the carbonate ion, and its slight positional disorder as seen by the behavior of the *c/a* ratio and unit cell volume (Bischoff et al., 1985). No relationship was found between *c/a* ratios, unit cell volumes, and the halfwidths of the calcites in this study. However, the range of halfwidths of ν_1 examined may have been too small to recognize any trend.

Future Research

The use of LRM to make routine measurements of $\delta^{18}O$ in calcite at the level of other current microbeam techniques is contingent on accurate and precise measurements of the intensity ratio of ν_1^*/ν_1. The accuracy and precision of measurements of the intensity ratio of ν_1^*/ν_1 are limited by: 1) resolving the ν_1^* and ν_1 peaks; 2) removal of Mn^{2+} fluorescence background; 3) variances in peak intensities governed by counting statistics. Future research should focus on limiting these three factors. Difficulties due to peak overlap can be minimized in many calcites by making measurements at low temperatures and by using a spectrometer with a highly dispersive grating and narrow entrance slit width. Both of these methods result in narrower Raman bands and allow the symmetric stretching band and its satellites to be clearly resolved for most samples. This is especially important in poorly crystalline and impure calcites where the peaks can be significantly wider (Bischoff et al., 1985). The complete elimination of Mn^{2+} fluorescence background in many calcites is not possible using the LRM measurement techniques outlined here. However, the use of an

alternate excitation wavelength may greatly reduce Mn^{2+} fluorescence in LRM spectra. Examination of the excitation spectrum of Mn^{2+} in calcite shows the 514 nm line of an Argon ion laser falls within an intense excitation (absorption) band (Figure 11). The 488 nm, 454 nm, and 363 nm lines of an Argon ion laser fall in much less intense excitation bands. Using these lines results in a substantial decrease in Mn^{2+} fluorescence in synthetic calcites (Pedone et al., 1990). However, these lines are less intense than the 514 nm line. The 488 nm line would offer the best compromise between intensity and Mn^{2+} excitation. Additional reduction of Mn^{2+} fluorescence background may be achieved by cooling the sample to near liquid helium temperatures. LRM measurements at these temperatures together with the use of the 488 nm, 454nm, or 363nm line may allow measurements to be made on a much larger range of natural calcites. The remaining limitation of making LRM oxygen isotopic measurements in calcites is that of counting statistics. Current multichannel detectors require acquisition times in excess of 24 hours to measure the ν_1^*/ν_1 intensity ratio in calcite with precisions of less than 1‰. The widespread use of LRM to make routine oxygen isotopic measurements in calcite probably cannot be realized without significant improvements in detector technology allowing significantly shorter integration times.

Conclusions

Both the $C^{18}O^{16}O_2^{2-}$ and $C^{17}O^{16}O_2^{2-}$ satellites to the $C^{16}O_3^{2-}$ symmetric stretching peak in calcite are easily observed in natural calcites at low temperatures. Attempting to use RMS oxygen isotopic values to "calibrate" LRM measurements of the intensity ratio of the ν_1^*/ν_1

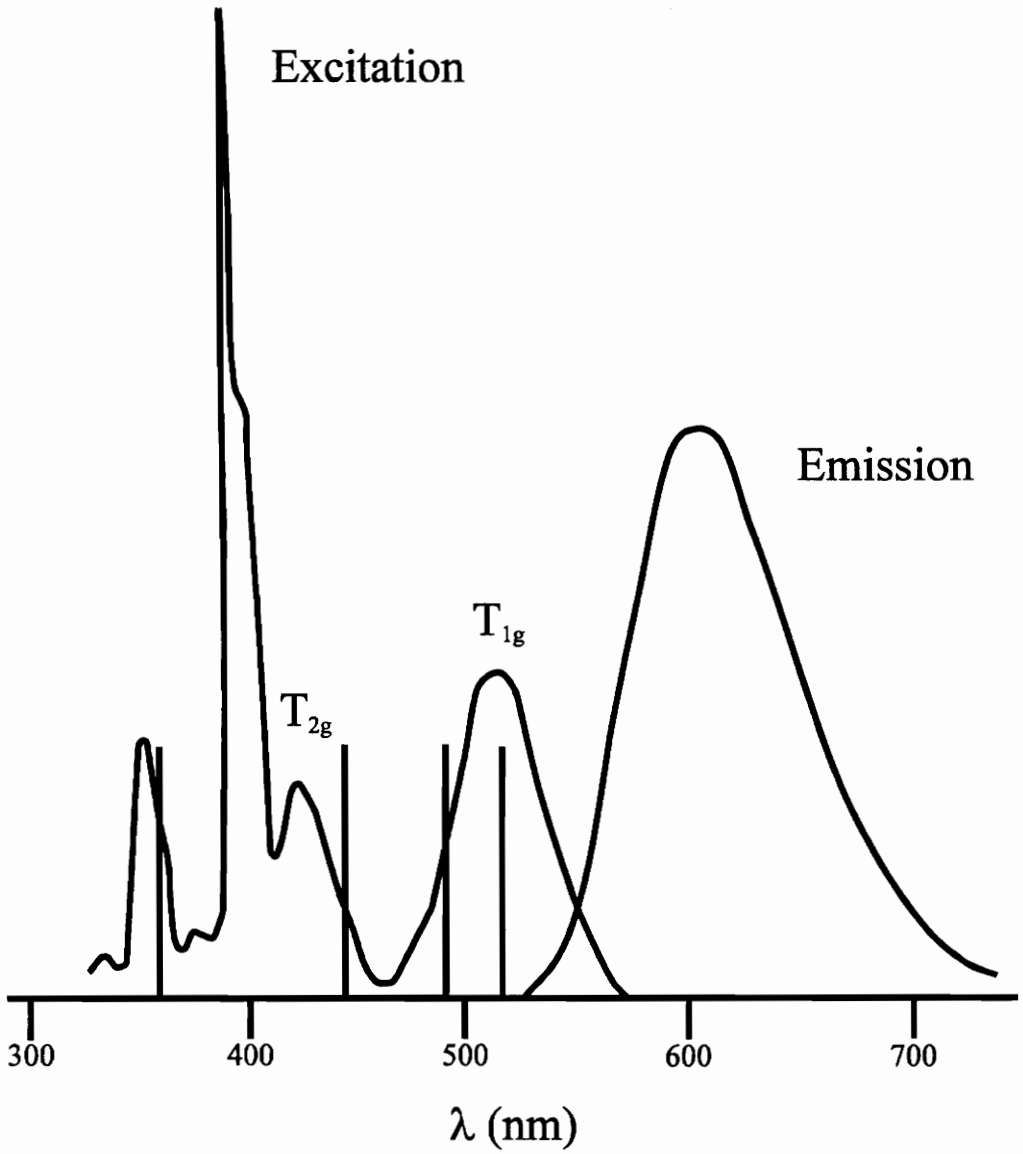

Figure 11: Excitation and emission spectra for Mn^{2+} in calcite (after Walker, 1985). The position of the lines of an Argon ion laser are superimposed for reference. Notice that the 514 nm laser line falls within a local excitation (absorption) maximum. This results in intense Mn^{2+} fluorescence emission.

peaks initially yielded poor results. However, the linear relationship between the difference between LRM and RMS isotopic values and the halfwidth of ν_1, allows correction of LRM $\delta^{18}O$ values to within 3.8‰ of RMS values. The main limiting factor in determining $\delta^{18}O$ of calcites by LRM is the background caused by Mn^{2+} fluorescence. Samples which are strongly fluorescent can contribute significantly to the background and error in measured LRM intensity ratios (Equation 7). At present the complete removal of Mn^{2+} fluorescence from LRM spectra by cooling the sample to near liquid-nitrogen temperatures is possible only in weakly fluorescent calcites. LRM measurements without Mn^{2+} fluorescence background may be possible on an even larger group of natural calcites by using laser excitation wavelengths that excite less fluorescence and by cooling the sample to near liquid helium temperatures.

While it is theoretically possible to make LRM isotopic measurements on weakly fluorescent calcites at the level of other microprobe techniques (i.e. <1‰), the precision and accuracy of LRM measurements is governed by counting statistics. LRM analyses would require acquisition times in excess of 24 hours to reach this level of precision and accuracy. This limitation will probably require significant improvements in detector technology before routine oxygen isotopic measurements in calcite can be achieved using LRM.

Appendix I

Sample ID	a (Å)	c (Å)	V (Å^3)
C60686	4.9907(2)	17.0642(9)	368.09(3)
HB659	4.9901(2)	17.065(9)	368.00(2)
OB001	4.9909(4)	17.071(2)	368.25(6)
SF0232	4.9893(3)	17.063(1)	367.84(4)
SYN5	4.9912(8)	17.071(4)	368.29(1)
SYN6	4.9886(7)	17.063(6)	367.72(1)
VPI001	4.9896(3)	17.064(1)	367.92(4)

Table 2: Cell parameters determined by powder X-ray diffraction for the natural and synthetic calcites (SYN5,6) in this study.

Sample ID	$\delta^{18}O$ (‰, SMOW)	Average $\delta^{18}O$ (‰,SMOW)
C60686	9.2, 9.2, 9.4	9.3
HB659	17.3, 17.6	17.4
OB001	14.9, 14.9, 15.0, 15.1	15.0
SF0232	23.2, 22.9	23.0
SYN5	23658.9	23658.9
SYN6	6258.8	6258.8
VPI001	18.6, 18.6	18.6

Table 3: Bulk $\delta^{18}O$ values determined by ratio mass spectrometry (RMS) for the natural and synthetic calcites (SYN5,6) in this study.

Sample ID	ν_4	ν_2	ν_3
C60868	712.3	875.7	1423.7
HB659	712.3	876.0	1426.6
OB001	712.6	876.5	1437.7
SF0232	712.7	876.5	1433.8
SYN5	711.6	874.5	1419.8
SYN6	711.5	874.8	1420.5
VPI001	712.3	875.8	1423.6

Table 4: Positions of the internal infrared-active vibrational bands for the calcites in this study. Positions have errors of 0.1 cm^{-1}, 3s.

Sample ID	T	L	ν_4	ν_1*	ν_1	ν_3	$2\nu_2$
C60868	155.3	282.0	712.5	1066.4	1086.3	1435.9	1748.9
HB659	154.3	280.6	711.7	1065.6	1085.3	1435.1	1748.2
OB001	155.4	281.7	712.5	1066.3	1086.3	1436.0	1749.1
SF0232	155.7	281.8	712.1	1066.2	1086.1	1435.5	1748.0
SYN5	154.5	280.8	712.1	1066.4	1086.0	1435.0	1748.8
SYN6	152.8	278.2	712.4	1065.9	1085.8	1433.9	1749.9
VPI001	153.9	280.2	711.6	1065.6	1085.4	1435.2	1748.3

Table 5: Positions of the Raman-active vibrational bands for the calcites in this study. Positions have errors of 0.2 cm^{-1}, 3s.

Appendix II

A Peak Fitting Method for Determining Reproducible Intensities of the Symmetric Stretching Bands in the Raman Spectrum of Calcite

Due to the large difference between the intensities of the symmetric stretching band and its satellites, it was necessary to fit the Raman spectra in multiple steps. First, the baseline was removed using the program SPLINE.AB in the Spectra Calc™ version 2.2 software. Control points were chosen *on* the spectrum with a nearly equal spacing of approximately 35 cm^{-1} around the symmetric stretching bands. For example, points were chosen at 928, 954, 989, 1010, 1147, 1192, 1240, and 1276 cm^{-1}. The program then fit a cubic spline to these points. If the fit appeared satisfactory, the fit spline-line was subtracted from the spectrum. Second, the $C^{16}O_3^{2-}$ peak was fit using the program FIT.AB (Square Tools™ utilities package) and subtracted from the spectrum. The $C^{16}O_3^{2-}$ peak was selected using the autopeak option and the minimum fullwidth at half maximum was set to be 2 cm^{-1}. The peak model was chosen to be a sum of Gaussian plus Lorentzian characters. The Voigt, Lorentzian, Gaussian, and product Gaussian and Lorentzian models resulted in significantly poorer fits of the spectra. All of the parameters including width, height, center, area, and fraction of Lorentzian character were allowed to be optimized. The fraction of Lorentzian character was the same within error for the symmetric stretching bands in each spectrum; however, the fraction of Lorentzian character ranged from 0.2 to 0.7 between spectra. No background parameters were

included in the fit. The model was then iterated until the χ^2 parameter reached convergence. At this time the residual was examined to determine any areas which had significant misfit (i.e. large residuals relative to the intensity of a nearby band). If the fit resulted in noticeable near the weakly symmetric stretching satellite bands the process was restarted. The resulting fit spectrum was then subtracted from the raw spectrum minus the background. This resulted in a spectrum with the $C^{18}O^{16}O_2^{2-}$ and $C^{17}O^{16}O_2^{2-}$ peaks isolated from the intense $C^{16}O_3^{2-}$ peak. Third, the $C^{18}O^{16}O_2^{2-}/C^{17}O^{16}O_2^{2-}$ peaks were then fit using the same procedure as the $C^{16}O_3^{2-}$ peak, except that an offset background term was added to the fitting procedure. The program reported optimized peak centers, halfwidths (full width at half maximum), areas, heights, and fraction of Lorentzian character. To minimize errors introduced by the fitting process each spectrum was fit three times and the average intensities were used to calculate intensity ratios.

References

Adar, F. (1981) Developments in Raman microanalysis. *Microbeam Analysis*, 67-72, 1981.

Bischoff, W.D., Sharma, S.K., and Mackenzie, F.T. (1985) Carbonate ion disorder in synthetic and biogenic magnesian calcites: a Raman spectral study. *American Mineralogist*, **70**, 581-589.

Bowen, R. (1988) *Isotopes in the earth sciences*. Elsevier Applied Science, 647 pp.

Burruss, R.C., Ging, T.G., and Knight, C.L. (1990) Multichannel Raman microprobe observations of $^{18}O/^{16}O$ in calcite; feasibility of $\delta^{18}O$ measurements with 3μm spatial resolution. *Eos, Transactions of the American Geophysical Union*, **71**, (43), 1655.

Burruss, R.C., Ging, T.G., and Carlson, D. (1989) Raman microprobe observations of carbon and oxygen stable isotopes in geologic materials. *Microbeam Analysis*, 173- 175, 1989.

Cloots, R. (1991) Raman spectrum of carbonates $M^{II}CO_3$ in the 1100-1000 cm^{-1} region: observations of the ν_1 mode of isotopic $(C^{16}O_2{}^{18}O)^{2-}$ ion. *Spectrochimica Acta*, **12**, 1745-1750.

Decius, J.C. (1955) Coupling of the out-of-plane bending mode in nitrates and carbonates of the aragonite structure. *Journal of Chemical Physics*, **23**, 1290-1294.

Decius, J.C. (1954) Isotope shift of the perpedicular bending frequency in KNO_3 and $NaNO_3$. *Journal of Chemical Physics*, **22**, 1941.

Dhamelincourt, P., Beny, J.M., Dubessy, J., and Poty, B. (1979) Anlyse d'inclusions fluides à la a microsonde MOLE à effet Raman: *Bulletin de Minealogie*, **102**, 600-610.

Diem, M. (1994) *Introduction to modern vibrational spectroscopy*. John Wiley & Sons, 285 pp.

Dickson, J.A.D., Smalley, P.C., Råheim, A., and Stijfhoorn, D.E. (1990) Intracrystalline carbon and oxygen isotope variations in calcite revealed by laser microsampling. *Geology*, **18**, 809-811.

Effenberger, H., Mereiter, K. Mereiter, and Zemann, J. (1980) Crystal structure of magnesite, calcite, rhodochrosite, siderite, smithsonite, and dolomite, with discussion of some aspects of the sterochemistry of calcite type carbonates. *Zeitschrift für Krystallographie*, **156**, 233-243.

Erickson, C.L., Bodnar, R.J., and Burruss, R.C. (1991) $\delta^{18}O$ analysis of calcites by Raman microprobe: effects of crystal chemistry. GSA Annual Meeting, Abstracts with Programs, **23**, A101.

Frech, R. and Decius, J.C. (1970) Dipolar coupling and molecular vibrations in crystals. IV. frequency shifts and dipole moment derivatives. *Journal of Chemical Physics*, **54**, 2374-2379.

Hurlbut, C.S. and Klein, C. (1977) *Manual of Mineralogy*, 19th ed., John Wiley & Sons: New York, 532 p.

Herzberg, G. (1945) *Infrared and Raman spectra of polyatomic molecules: molecular spectra and molecular structure II.* D. Van Nostrand Co., inc., 632 pp.

Hirschfeld, T. (1982) Microspectroscopy, *Microbeam Analysis*, 1982, 247.

Krishnamurti, D. (1957) The Raman spectrum of calcite and its interpretation. Memoir No. 100 from the Raman Research Institute, Bangalore-6, 183-209.

Long, D.A. (1977) *Raman spectrometry*. McGraw-Hill, 276 pp.

Malyj, M. and Griffiths, J.E. (1983) Stokes/Anti-Stokes Raman vibrational temperatures: reference materials, standard lamps, and spectrophotometric calibrations. *Applied Spectroscopy*, **37**, 315-333.

Mook, W.G. (1971) Paleotemperatures and chlorinities from stable carbon and oxygen isotopes in shell carbonate. *Palaeogeogr. Palaeoclimatol. Palaeocol.*, **9**, 4, 245-263.

O'Neil, J.R. and Clayton, R.N. (1964) Oxygen isotopic geothermometry. In: *Isotopic and Cosmic Chemistry*. H. Craig, S. Miller, and G. Wasserburg, eds., North-Holland, Amsterdam, 157-168.

Park, K. (1966) New width data of the A_{1g} Raman line in calcite. *Physics Letters*, **22**, 39-41.

Pasteris, J.D., Wopenka, B., and Seitz, J.C. (1988) Practial aspects of quantitative laser Raman microprobe spectroscopy for the study of fluid inclusions: *Geochimica et Cosmochimica Acta*, **52**, 979-988.

Pedone, V.A, Cercone, K.R., and Burruss, R.C. (1990) Activators of photoluminescence in calcite: evidence from high-resolution, laser-excited luminescence spectroscopy. *Chemical Geology*, **88**, 183-190.

Placzek, G. (1934) Rayleigh-Streuung and Ramaneffekt, *in* Marx, E., ed., *Handbuch der Radiologie*, **6**, pt.2: Leipzig, Akademische Verlagsgesellschaft, 205-374.

Riciputi, L.R., and Patterson, B.A. (1994) High spatial-resolution measurement of O isotope ratios in silicates and carbonates by ion microprobe. *American Mineralogist*, **79**, 1227-1230.

Rosasco, G.J. et al., (1975) Laser-excited Raman spectroscopy for nondestructive partial analysis of individual phases in fluid inclusions in minerals. *Science*, **190**, 600-610.

Seitz, J.C., Pasteris, J.D., and Chou, I. (1993) Raman spectroscopic characterizations of gas mixtures. I. quantitative composition and pressure determinants of CH_4, N_2, and their mixtures. *American Journal of Science*, **293**, 297-321.

Sheppard, S.M.F. and Taylor, H.P., Jr. (1974) Hydrogen and oxygen isotope evidence for the origins of water in the Boulder Batholith and Butte ore deposits, *Montana Economic Geology*, **69**, 926-946.

Smalley, P.C., Stifjhoorn, D.E., and Råheim, A., Johansen, H., and Dickson, J.A.D. (1989) The laser microprobe and its application to the study of C and O isotopes in calcite and aragonite. *Sedimentology Geology*, **65**, 211-221.

Strommen, D.P. and Nakamoto, K. (1984) *Laboratory Raman spectroscopy*. Wiley-Interscience, 134pp.

Valley, J.W., H.P. Taylor, Jr., and O'Neil, J.R. *eds.*, *Stable Isotopes in High Temperature Geologic Processes*. Mineralogical Society of America, 570pp.

Viezer, J. (1983) Trace elements and isotopes in sedimentary carbonates, in *Carbonates: mineralogy and chemistry*, Reeder, R.J., *ed.*, 265-299.

Walker, G. (1985) Mineralogical applications of luminescence techniques. In: F.J. Berry and D.J. Vaughan, Eds., Chemical Bonding and Spectroscopy in Mineral Chemistry. Chapman and Hall, London, 103-140.

Walker, G., Abumere, O.E., and Kamaluddin, B. (1989) Luminescence of Mn^{2+} centres in rock-forming carbonates. *Mineralogical Magazine*, **53**, 201-211.

White, W.B. (1974) The carbonate minerals. In V.C. Farmer, Ed., *The infrared spectra of minerals*. Mineralogical Society Monograph 4, 227-284. Mineralogical Society, London.

Vita

Scott Mutchler was born on May 10, 1970 in Phillipsburg, New Jersey. He spent most of his youth in Easton, Pennsylvania. From an early age he knew that he wanted to become a geologist. At the age of 16 his family moved to Lower Mount Bethel, Pennsylvania where he attended Bangor Area High School. At this time, he found a new interest in chemistry, physics, and computers. Upon graduation he attended Indiana University of Pennsylvania where he studied the Geological Sciences. He earned his Bachelor of Science degree in Geological Sciences and was accepted into the graduate program at Virginia Polytechnic Institute and State University in the spring of 1993. He completed a Masters of Science in Geological Sciences in the spring of 1995.